


Vázquez, Aldo ; Castro-Carranza, Alejandra ; Rodríguez, Mario Alejandro Carrizales ; Maldonado, José Luis ; Castro-Chacón, Andres ; García-González, Leandro ; Hernández-Torres, Julián ; 

Numerical study of efficient ternary planar hybrid solar cells using simple boron molecules as organic compounds

Journal Article as: peer-reviewed accepted version (Postprint)

DOI of this document* (secondary publication): <https://doi.org/10.26092/elib/3691>

Publication date of this document: 17/02/2025

* for better findability or for reliable citation

Recommended Citation (primary publication/Version of Record) incl. DOI:

A. Vázquez, A. Castro-Carranza, M. Rodríguez, J.L. Maldonado, A. Castro-Chacón, L. García-González, J. Hernández-Torres, J. Martínez-Castillo, L. Zamora-Peredo, J. Gutowski, J.C. Nolasco, Numerical study of efficient ternary planar hybrid solar cells using simple boron molecules as organic compounds, *Optical Materials*, Volume 132, 2022, 112852, ISSN 0925-3467, <https://doi.org/10.1016/j.optmat.2022.112852>.

Please note that the version of this document may differ from the final published version (Version of Record/primary publication) in terms of copy-editing, pagination, publication date and DOI. Please cite the version that you actually used. Before citing, you are also advised to check the publisher's website for any subsequent corrections or retractions (see also <https://retractionwatch.com/>).

This document is made available under a Creative Commons licence.

The license information is available online: <https://creativecommons.org/licenses/by-nc-nd/4.0/>

Take down policy

If you believe that this document or any material on this site infringes copyright, please contact publizieren@suub.uni-bremen.de with full details and we will remove access to the material.

Numerical study of efficient ternary planar hybrid solar cells using simple boron molecules as organic compounds

A. Vázquez^a, A. Castro-Carranza^{b,c}, M. Rodríguez^d, J.L. Maldonado^d, A. Castro-Chacón^b,
L. García-González^a, J. Hernández-Torres^a, J. Martínez-Castillo^a, L. Zamora-Peredo^a,
J. Gutowski^{c,e}, J.C. Nolasco^{a,*}

^a Micro and Nanotechnology Research Centre MICRONA, Veracruz University, 94294, Veracruz, Mexico

^b International Laboratory of Environmental Electron Devices (LAIDEA UNAM), ENES Morelia, National Autonomous University of Mexico, 58190, Morelia, Mexico

^c Semiconductor Optics, Institute of Solid-State Physics, University of Bremen, 28359, Bremen, Germany

^d Research Group of Optical Properties of Materials (GPOM), Centro de Investigaciones en Optica A.C., A.P. 1-948, 37000, León, Guanajuato, Mexico

^e MAPEX Center of Materials and Processes, University of Bremen, 28359, Bremen, Germany

ARTICLE INFO

Keywords:

Boron compounds
Numerical simulations
Ternary organic solar cells
Density of trap states
Optimized thickness
Energy band diagrams

ABSTRACT

Ternary solar cells have proven to be a solution to absorb more photons at different wavelengths and reduce the recombination of charge carriers. Here, we propose a new hybrid organic-inorganic ternary planar solar-cell structure using a novel boron compound. The role of this material on the performance of the device with a polymer/borinate/ZnO configuration is studied. As the donor polymer, we evaluate P3HT, PTB7, and PCPDTBT; and three boron compounds with different properties, especially concerning the bandgap and trap energy depth. To validate the experimental electrical characteristics of the borinates, first, we simulate a bilayer structure with C₆₀, subsequently, we simulate and analyze the whole device architecture. The ternary solar cell with PTB7 and a borinate with a bandgap of 1.66 eV and a medium trap energy depth of 0.95 eV above the HOMO level exhibit the highest efficiency, i. e. 11.7%. Furthermore, we present a layer thickness optimization of the materials to reach even higher efficiencies, up to 15.15%. Finally, the effect of the magnitude of the density of trap states in the borinate on the device performance is analyzed.

1. Introduction

Organic solar cells (OSCs) are a viable and sustainable alternative of around less than one-third of the costs of polycrystalline silicon cells [1] due to the relatively cheap materials and low processing temperatures used. The current power conversion certified efficiency (PCE) of this type of solar cell has been reported to reach up to 18% [2]. To achieve this, the types of OSC architectures have played a fundamental role in the optimization of their photovoltaic (PV) parameters [3]. Among the different architectures reported in the literature [4,5], the bilayer planar heterojunction consists of an organic donor semiconductor (D) and an acceptor one (A), which dissociate the electron-hole pair formed by the absorbed sun photons at the semiconductor materials of the device. The bilayer planar configuration has reached efficiencies as high as 16% [6]. However, both the diffusion length of the free charge carriers and the low heterojunction interfacial area limit this configuration [3]. The bulk

heterojunction architecture overcomes such limitations by blending donor and acceptor semiconductors before being deposited.

To increase the efficiency of the solar cell, architectures involving three or more materials have been proposed. One of them is the tandem solar cell configuration [7], which was initially proposed for inorganic solar cell technologies. This configuration consists of two or more junctions that efficiently absorb photons at different wavelength ranges allowing thus to cover the solar spectrum as complete as possible. However, the costs of production of the tandem technology limit the scalability of OSCs. Hence, a low-cost alternative regarding tandem architecture is the ternary OSCs which incorporate the third component into a binary bulk structure to increase photon collection. This results in a higher short-circuit current density (J_{SC}) and PCE while maintaining the simplicity of the single bulk junction architecture.

The selection of materials of the active layer must agree with two conditions to increase the PCE: i) the semiconductors must absorb as

* Corresponding author.

E-mail address: janolasco@uv.mx (J.C. Nolasco).

many photons as possible from the solar spectrum at different wavelengths to photo-generate a high density of electric charges [8]; ii) a proper energy level alignment to promote the separation and collection of charge carriers at their respective contacts [9]. In organic ternary solar cells, polymers P3HT and PTB7 as donors together with fullerenes as acceptors (C_{60} , C_{70} , and derivatives) have been extensively used as the main heterojunction [10,11]. For the third compound, the material can be a donor or acceptor. Small molecules, such as fullerene derivatives, have also been used, which contribute to both the collection of more photons and the extraction of more charge carriers through the contacts. However, fullerenes limit OSC PV parameters due to: i) their weak light absorption from the solar spectrum, ii) the functionalization difficulty to tune their bandgaps, and iii) their fast degradation when exposed to air [12]. An additional disadvantage of the fullerenes is their high costs because of the complex molecular structure; for example, the costs of $PC_{61}BM$ and $PC_{71}BM$ are around three times higher than those of P3HT [13]. Thus, an effort has been addressed to overcome these issues through the study of non-fullerene acceptors (NFA), which have resulted in high device performance and a low-cost material alternative in OSCs [14–17]. Specifically, Yan et al. [18] reported a PCE of 16% using Y6 as an NFA in a ternary solar cell structure. Further, Liu et al. [19] obtained an efficiency of 17.6% using a D18:Y6 solar cell structure, where D18 is a small-molecule organic semiconductor. Also, by designing and synthesizing an NFA, Li et al. [17] reached a PCE of 18% with a configuration of PM6:L8-BO (2-butyloctyl substitution). Recently, an efficiency of 19% was achieved by using an NFA named eC9-2Cl [20]. However, the synthesis of materials such as Y6, D18, PM6, L8-BO, and eC9-2Cl can be relatively complex if compared with more simple molecules such as the boron compounds since the former materials require more step synthesis, which increases the production costs of solar cells [21,22].

Boron compounds have been widely studied for solar cells due to their simple fabrication process and tunable properties. The boron compounds can be classified into different types, such as boron dyrromethenes (BODIPYs) [17,22,23], boron-containing subphthalocyanines [24], and borinates [25–27]. These compounds have been usually used in organic binary solar cells [12,28,29]. In this work, we propose for the first time a novel ternary solar cell structure using borinates as the third non-fullerene compound, demonstrating efficiencies in the order of the ones reported in the literature for such kind of devices but using more complex molecules.

First, we present a calibration based on previously fabricated borinate/ C_{60} bilayer solar cells to validate the optical and electrical characteristics of the boron compounds under study, i.e., called B1, B2, and B3 with different properties (for details, see Table 1). Second, nine different hybrid planar solar cell configurations are explored using three of the most studied p-type polymers in literature (P3HT, PTB7, and PCPDTBT), organic borinates as the third compound, and ZnO as the n-type counterpart. Third, the efficiency of the solar cell configuration is optimized by varying the thickness of its layers. Finally, the effect of the variation of the borinate trap density of states on the solar cell performance is analyzed.

2. Methodology

2.1. Calibration of the organic boron compound parameters

To calibrate the electrical parameters of the borinates analyzed in this work, i.e., B1, B2, and B3 (Fig. 1 shows molecular structures of borinates), their experimental characteristics including EQE curves from previously fabricated and reported borinate/ C_{60} bilayer solar cells [21] were modeled using the software AFORS-HET. This software is a tool that solves the one-dimensional semiconductor equations that govern the electrical behavior of solar cells, e.g. Poisson's equation, charge generation, transport and continuity equations [30]. As borinate fitting parameters, we used the following: electron affinity, the thickness, and the trap density of states (tDOS). This method is usually applied to

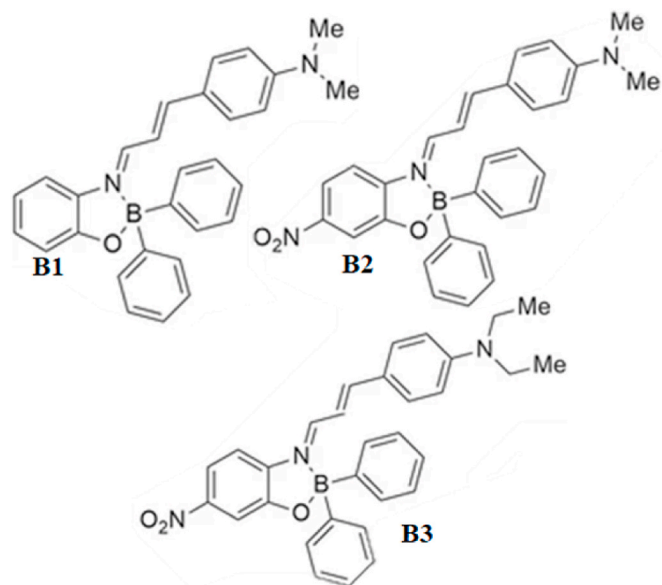


Fig. 1. Molecular structure of borinates.

determine the parameters of materials applied in OSCs through the validation of simulations with experimental measurements [31]. For this purpose, similar values to the measured ones were used for the thickness and electron affinity, considering the tolerance of the respectively used techniques. In the case of the tDOS, to our knowledge, there are no values for borinates reported in the literature, thus, this and the tDOS in the fullerene are our free fitting parameters. The tDOS for both borinates and polymers is considered to be caused by acceptors since in organic semiconductors the non-intentional doping has been attributed to acceptor tDOS [32]. The parameters of C_{60} which is a well-known material were taken from literature (see Table 1). C_{60} tail states are considered [33,34]. Reported studies on conduction mechanisms in organic heterojunctions indicate recombination at either the bulk region of the materials or the interface (semiconductor/semiconductor or semiconductor/metal). The recombination occurring at the organic semiconductor/semiconductor interface can be described by tunneling enhanced interface recombination [35,36]. Such recombination can take place through trap states that can be localized either at the interface or within the materials. Thus, for simplicity, all the interfaces were considered to be ideal. The reported and extracted physical parameters of both the boron compounds and the C_{60} are listed in Table 1.

2.2. Simulation details of the proposed structure

The structure of the ternary cells consists of a donor/donor/acceptor (polymer/borinate/ZnO) planar configuration (Fig. 2a). Taking into account their relative high absorption coefficients, the selected polymers were P3HT (poly [3-hexylthiophene]), PTB7 (poly [[4,8-bis [(2-ethylhexyl)oxy]benzo[1,2-b:4,5-b']dithiophene-2,6-diyl][3-fluoro-2-[(2-Ethylhexyl)carbonyl]thienc[3,4-b]thiophenediyl]]), and PCPDTBT (poly[2,6-(4,4-bis-(2-Ethylhexyl)-4H-cyclopenta[2,1-b; 3,4-b']dithiophene)-alt-4,7(2,1,3-enzothiadiazole)]) [12]. The electrical parameters of the polymers and ZnO are shown in Table 2. ZnO is proposed as an electron acceptor due to its appropriate energy band levels (with regard to the borinates) to increase the charge extraction [41]. This will be discussed in detail later. Besides, the fabrication of ZnO is relatively of low cost. Current density-voltage (J - V) curves of nine combinations of these solar cell constituents using the mentioned materials (as specified in Table 3) were simulated under AM 1.5 illumination. The isolated energy levels of the materials and the expected routes of the photo-generated charges are also indicated in Fig. 2b.

The absorption coefficient spectra of both polymers and boron

Table 1Physical parameters used for the simulation of boron compounds and fullerene C₆₀.

Semiconductors	B1	B2	B3	C ₆₀
Thickness (nm)	12	17	10	32–38
Dielectric constant, ϵ_r	4 [37]	4 [37]	4 [37]	3 [37]
Electron affinity, X (eV)	3.4	3.4	3.4	3.6
Bandgap, E_g (eV)	1.75 [21]	1.56 [21]	1.66 [21]	2.3 [38]
Optical Bandgap, $E_{g \text{ opt}}$ (eV)	1.75 [21]	1.66	1.72 [21]	2.3 [38]
Effective conduction band density, N_c (cm ⁻³)	10 ²¹	10 ²¹	10 ²¹	10 ²¹
Effective valence band density, N_v (cm ⁻³)	10 ²¹	10 ²¹	10 ²¹	10 ²¹
Effective electronic mobility, μ_n (cm ² /Vs)	10 ⁻³	10 ⁻³	10 ⁻³	0.1 [39]
Effective hole mobility, μ_p (cm ² /Vs)	10 ⁻³	10 ⁻³	10 ⁻³	0.1 [39]
Doping concentration acceptors, N_a (cm ⁻³)	0	0	0	0
Doping concentration donors, N_d (cm ⁻³)	0	0	0	10 ¹⁸ [40]
Total trap density, N_t (cm ⁻³)	10 ¹¹ , Acceptor, Gaussian 1.12 eV above E_v	10 ¹¹ , Acceptor, Gaussian 0. 6 eV above E_v	10 ¹¹ , Acceptor, Gaussian 0.95 eV above E_v	10 ¹⁶ , Acceptor, tails type states

compounds taken from the literature are shown in Fig. 3. As a reference, the solar spectrum AM1.5 (which corresponds to the input energy) is also depicted in the same figure. Note that the B3 borinate is the material with the highest absorption when compared to B1 and B2. The P3HT and PTB7 polymers show each one absorption peak at 520 and 670 nm, respectively, whereas PCPDTBT exhibits two maximum absorptions maxima, one at 400 nm and one at 650 nm. Thus, since all the polymers show absorption bands being somewhat complementary to those of the different borinates, we study all possible combinations among materials to find the optimum covering of AM1.5 and thus the highest efficiency.

To further increase the efficiency of a solar cell, the thickness of its ingredient layers has to be optimized. For this purpose, with regard to the here studied combinations, the thickness of each layer was varied in

a range between 10 and 130 nm to find the optimum.

The tDOS in semiconductors induces enhanced charge carrier recombination. These defects can originate from either chemical impurities introduced during synthesis and the device fabrication process (extrinsic defects), and/or by covalent and non-covalent bondings (intrinsic defects) [50]. Thus, for a more complete analysis, the effect of the total tDOS in the borinate B3, which showed the most efficient performance in the devices, was studied. The tDOS was varied from 10⁹ to 10¹² cm⁻³, which is a range typically reported for organic solar cell simulations [31,46].

3. Results and discussion

Fig. 4 (a) shows the experimental and simulated external quantum efficiency (EQE) curves. The experimental and simulated J - V under illumination is depicted in Fig. 4 (b). It can be observed a reasonably good agreement between experimental data and our numerical simulation results for both J - V and EQE characteristics. Such matching is comparable with others of the same type reported in the literature [51–53]. The slight differences between experimental and simulated characteristics found here can be attributed to experimental issues, i. e. to the difference in the uniformity of illumination beam or to the difference in exactly positioning the same device area through the used mask between the two used techniques, which given raised to slightly differences on the generated photocurrent [54,55]. For borinates, the agreement was achieved using trap densities of 10¹¹ cm⁻³ located at 1.12 eV, 0.6 eV, and 0.95 eV for B1, B2, and B3, respectively, as shown in Table 1. To our knowledge, those values have not been reported before. The used calibrated parameters, i.e., electron affinity and bandgap, of borinates (B1, B2, B3) are in reasonable agreement with the ones reported in the literature using experimental techniques [21] as specified in Table 1.

Table 3 shows the PV parameters obtained from the J - V curves under illumination of the nine non-optimized devices resulting from combining the 3 polymers and the 3 borinates. With the aim to compare the performance of such combinations, the thickness of all devices was fixed to the same values of around 20 nm. Note that all ternary solar cells are functional and show efficiencies from 1.5 to 11.7%. Among borinates, B3 becomes the best alternative due to its highest absorption compared to B1 and B2 (Fig. 2). Borinate B2 shows PV parameters close to the ones obtained using B3; the efficiency difference between both B3 and B2 using PTB7 was 2%, which can be attributed to the noticeable difference in absorption [56].

Hence, among the three borinates, PTB7/B3/ZnO solar cells show the highest efficiency of 11.7%. These values are similar to the 11.8% efficiency reported by Usmani et al. [57] and 10.2% reported by Zhou et al. [58] but using structures based on fullerenes, i. e. PTB7-th:PCBM: ZnO. This can be understood on the basis of the two conditions

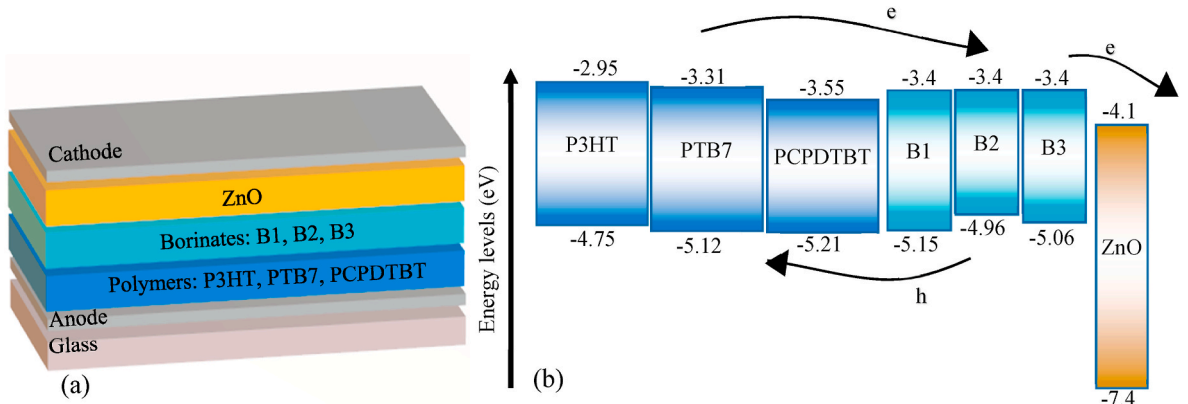


Fig. 2. (a) Device structure and (b) energy band levels before contacting expected routes for photogenerated electrons and holes are schematized.

Table 2

Physical parameters used for the simulation of polymers and ZnO.

Semiconductor	P3HT	PTB7	PCPDTBT	ZnO
Thickness (nm)	50	50	50	50
Dielectric constant, ϵ_r	6.65 [37]	3.4 [42]	4 [37]	9 [43]
Electron affinity, X (eV)	2.95 [44]	3.31 [45]	3.55	4.1 [46]
Band gap, E_g (eV)	1.8 [44]	1.81 [45]	1.66 [21]	3.3 [46]
Optical Band gap, $E_{g\ opt}$ (eV)	1.8 [44]	1.81 [45]	1.72 [21]	3.3 [46]
Effective conduction band density, N_c (cm ⁻³)	10 ²¹	10 ²¹	10 ²¹	4 x 10 ¹⁸ [46]
Effective valence band density, N_v (cm ⁻³)	10 ²¹	10 ²¹	10 ²¹	10 ¹⁹ [46]
Effective electronic mobility, μ_n (cm ² /Vs)	0.1	1x10 ⁻³	0.02	100 [43]
Effective electronic mobility, μ_p (cm ² /Vs)	0.1	1x10 ⁻³	0.02	25 [43]
Doping concentration acceptors, N_a (cm ⁻³)	0	0	0	0
Doping concentration donors, N_d (cm ⁻³)	0	0	0	2 x 10 ¹⁶
Total trap density, N_t (cm ⁻³)	2 x 10 ¹⁶ Acceptor, tails type states [44]	10 ¹⁵ Acceptor, tails type states [47]	10 ¹⁶ Acceptor, tails type states [32]	2 x 10 ¹⁷ Donor, uniform, 1.7eV above E_v [46]

Table 3

Photovoltaic parameters of polymer/borinate/ZnO structures.

Configuration	J_{SC} (mA/cm ²)	V_{OC} (V)	FF (%)	PCE (%)
P3HT/B1/ZnO	5.1	1.15	25.6	1.5
PTB7/B1/ZnO	12.5	1.37	46.4	7.9
PCPDTBT/B1/ZnO	11.7	1.15	28.0	3.8
P3HT/B2/ZnO	5.7	1.12	35.2	2.3
PTB7/B2/ZnO	12.1	1.30	61.8	9.7
PCPDTBT/B2/ZnO	11	1.15	65.5	8.3
P3HT/B3/ZnO	6.9	1.15	33.3	2.7
PTB7/B3/ZnO	13.4	1.35	66.9	11.7
PCPDTBT/B3/ZnO	13.8	1.15	60	9.5

previously stated in the introduction to increase the PCE regarding the selection of the active layer materials, i.e., i) PTB7 and P3HT absorb more photons than the PCPDTBT [59]. Specifically, it causes an increment of the photocurrent according to the general J_{SC} equation (Eq. (1)) where q is the charge of the electron, $EQE(\lambda)$ is the external quantum efficiency, $N_{ph}(\lambda)$ is the photon flux density in the AM 1.5 spectrum. The $EQE(\lambda)$ is directly related to the absorption coefficient; ii) The difference between PTB7 and P3HT can be explained by a higher built-in electric field in the device that promotes the separation and collection of charge carriers at their respective contacts [36,60,61]. This phenomenon will be discussed later in detail.

$$J_{SC} = \int_{AM1.5} q * EQE(\lambda) * N_{ph}(\lambda) d\lambda \quad (1)$$

The variation efficiency between the B1 structure and the B2 one was

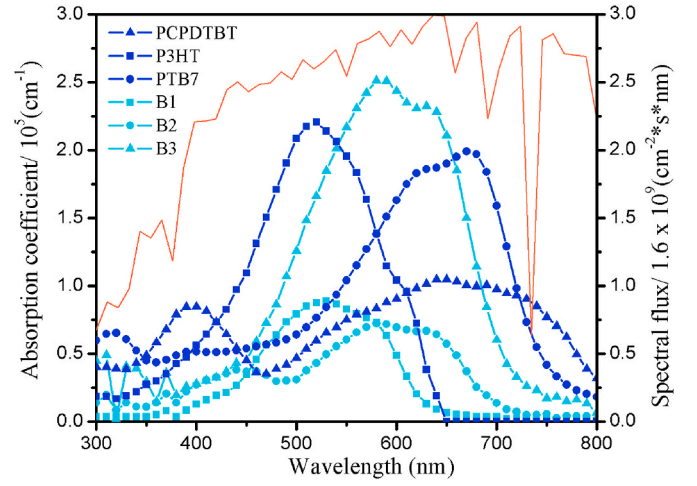


Fig. 3. Spectra of absorption coefficients of borinates [21], and polymers [48, 49] overlapped with the photon flux of the AM 1.5 solar spectrum (red solid line).

7.9–9.7% with B2 showing the highest value. This is attributed to an s-shape effect observed for the B1 solar cell structure, which can be noticed in Fig. 5, where J - V characteristics under illumination of PTB7/borinates (B1, B2, B3)/ZnO are depicted. In organic solar cells, this s-shape effect has been attributed to charge recombination occurring in either the materials or interfaces [62]. In our simulations, such an effect can be attributed to an increase of charge recombination within the materials due to the reduction of the built-in electric field, causing therefore a decrease in the FF (see Table 3).

Further, to understand the S-shape effect the band diagrams of the B1 and B2 devices were simulated. These diagrams under illumination and at the polarization of 0.65 V are shown in Fig. 6a and Fig. 6b. The 0.65 V condition is used since it is within the range where the S-shape effect was observed. Notice that the PTB7 energy bands in the B2 configuration (Fig. 6b) result in a band bending phenomenon, which improves the FF in comparison to the B1 case (Table 3). This is attributed to a higher electric field (due to a larger band bending) in the B2 configuration which reduces recombination with regard to the B1 case (Fig. 6a) where the bands are practically flat.

Fig. 7 shows the recombination rates versus the thickness of the devices under the same conditions as the band diagrams. Thus, one can observe the recombination behavior of the solar cell's materials under such specific conditions. By comparing both figures, the recombination in the PTB7 material decreases about 2 orders of magnitude, meanwhile, the one in B2 increases by about the same order. Since the PTB7 layer is thicker than the borinate one, it is expected that the recombination occurring in PTB7 is the predominant one. These facts can explain the origin of the S-shape effect considering that the band bending phenomena in organic semiconductor devices can promote charge extraction and thus, reduce charge recombination [63].

The solar cell configurations using the PCPDTBT as a polymer showed a maximum efficiency of 9.5% and electrical characteristics of J_{SC} and V_{OC} close to those of the PTB7-involving system. This makes the PCPDTBT polymer also a viable alternative. Among PCPDTBT-based solar cells, the lowest efficiency (3.8%) exhibited by the PCPDTBT/B1/ZnO structure agrees with that reported for a ternary device (3.65%) based on fullerenes (PCPDTBT:PCBM:ZnO) [64]; whereas the highest efficiency (9.5%) exhibited by the PCPDTBT/B3/ZnO structure agrees with that reported for a tandem cell (8.2%) based on two active layers composed of PCPDTBT:PCBM, and P3HT:PCBM [65].

Among the polymers used, the type of solar cell that shows the lowest efficiencies (1.5–2.7%) is the P3HT configuration. This value is between the 1.5% value reported by Poe et al. [66] and the 4.28% one reported by Zarkar et al. [67] using structures based on P3HT:BODIPY/ZnO. The

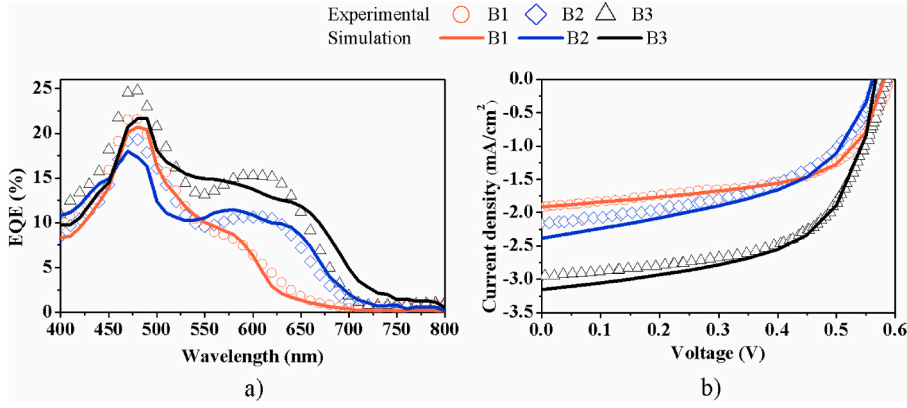


Fig. 4. Simulated and experimental curves: a) EQE and b) illuminated J-V characteristics.

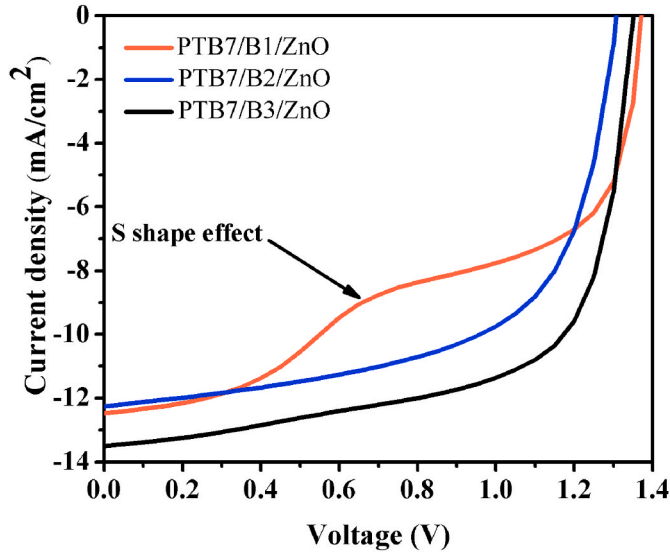


Fig. 5. Simulated J-V characteristics under illumination of PTB7/borinate (B1, B2, B3)/ZnO.

combination of P3HT and B3 exhibits one of the highest solar spectrum absorptions as can be noted in Fig. 2. This phenomenon can be understood using the simulated band diagrams depicted in Fig. 8. In this figure, notice that the bands of P3HT are practically flat (Fig. 8a), in contrast to those of PTB7 in Fig. 8b. Thus, the efficiency reduction can be also explained by an increment of recombination (see S1 and S2 in supplementary information).

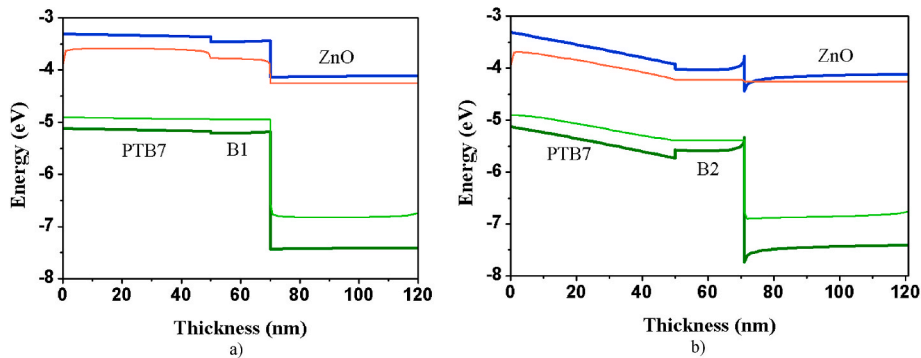


Fig. 6. Simulated band diagrams (the green/blue lines are the valence/conduction band, respectively) with quasi-Fermi levels of electrons (orange line) and holes (light green line) at a polarization of 0.65 V of (a) PTB7/B1/ZnO and (b) PTB7/B2/ZnO.

Fig. 9 shows the J-V characteristic (Fig. 9a) and the external quantum efficiency, EQE (Fig. 9b), for the optimized and non-optimized PTB7/B3/ZnO solar cell. In the following, we will rationalize the observed differences between an optimized and a non-optimized device based on the physics of the device. The photovoltaic parameters of the optimized device result in J_{SC} of 21 mA/cm², V_{OC} of 1.3 V, FF of 54.5%, and PCE of 15.15%. Among these parameters, the J_{SC} shows the largest increase by 8 mA/cm². This increase is due to the considerable rise of the photon absorption achieved by the thickness optimization (Fig. 9b) which will be discussed below. The slight V_{OC} reduction can be attributed to an increment of bulk trap states recombination due to the thicker layers in the optimized device [68]. The optimized PCE even exceeds reported values of 13.2% [69] and 13.4% [70] for organic solar cells using PTB7 and comes close to the efficiency record of 15.68% using a PTB7:PC71BM:EP-PDI configuration [71]. Thus, our proposed configuration is well viable to be fabricated.

In Fig. 10 the optimization process of the PTB7/B3/ZnO ternary solar cell is depicted. Both PTB7 and B3 show larger changes of their PV parameters as a function of thickness than ZnO. The highest light absorption of PTB7 and B3 can cause this sensibility. Notice that there exists a maximum PCE for each material at an optimal thickness, i. e., 100 nm for PTB7, 90 nm for B3, and 40 nm for ZnO. The maximum efficiency achieved is 15.15%, 3.85% below the record reached by Cui et al. [20] using a complex NFA (eC9-2Cl) as the third component in a TSC. However, our proposal to use B3 as the ternary material is a low-cost alternative [26,27] due to its facile synthesis, with around half of the synthesis process steps, when compared to those for a complex NFA [20,72,73].

The existence of optimized thicknesses is attributed to a trade-off between the increase of photon absorption and the reduction of charge recombination. The absorption is based on the Beer-Lambert

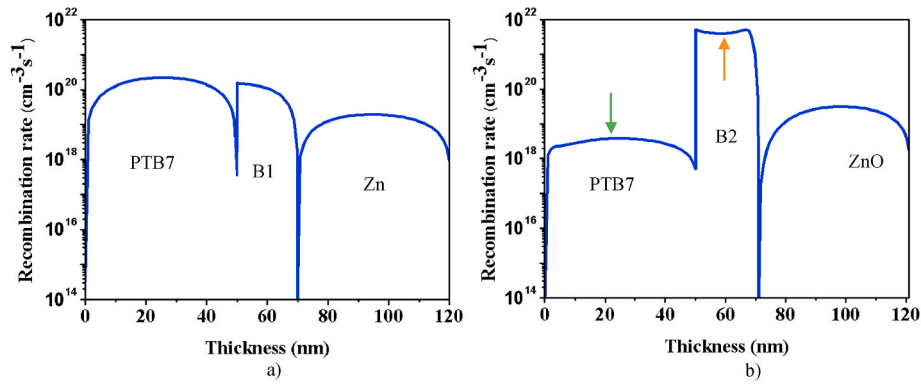


Fig. 7. Recombination rates at a polarization of 0.65 V of (a) PTB7/B1/ZnO and (b) PTB7/B2/ZnO.

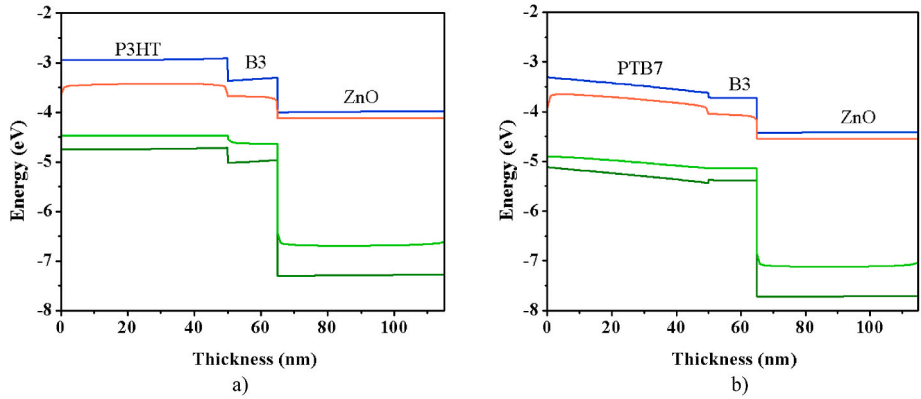


Fig. 8. Simulated band diagrams (the green/blue lines are the valence/conduction band, respectively) with quasi-Fermi levels of electrons (orange line) and holes (light green line) at the polarization of 0.35 V of (a) P3HT/B3/ZnO and (b) PTB7/B3/ZnO.

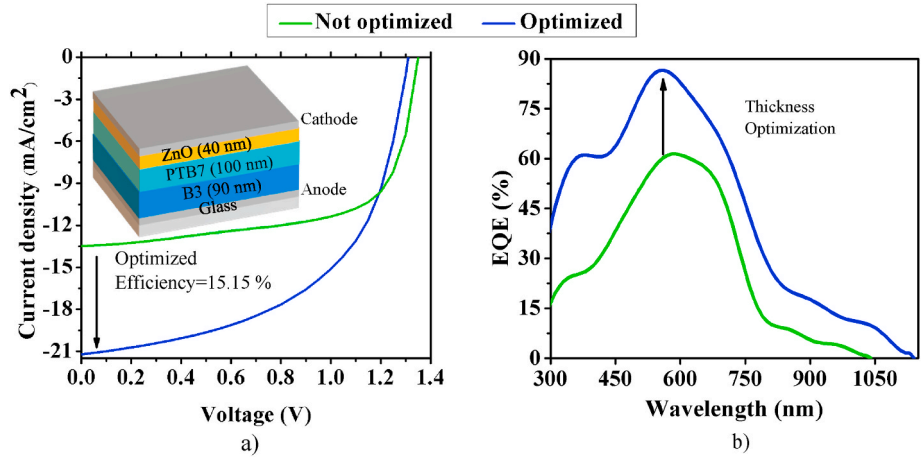


Fig. 9. (a) J-V curves of a non-optimized (green) and an optimized device structure (blue), (b) the EQE spectra as simulated under illumination of PTB7/B3/ZnO solar cells.

equation $A = 1 - e^{-\alpha l}$, with A the absorbance, α the absorption coefficient, and l the thickness. The increment of l improves the photocurrent which can be seen in Fig. 10. Meanwhile, the charge recombination reduction is caused by an electric field increment due to a thickness reduction, which can also explain the V_{OC} decrement observed in Fig. 9. Such an electric field variation and its effect on charge recombination, which in turns reduce the fill factor, can be observed in Fig. S3, supporting information. This figure depicts the band diagrams of three PTB7/B3/ZnO solar cells with different thicknesses of (a) PTB7, (b) B3,

and (c) ZnO, the thickness values being chosen around the optimal ones. The corresponding recombination rates are also shown in Fig. S3 (d-f). Notice that the reduction of the electric field for the largest PTB7 thickness causes an increment in the recombination. The same phenomenon is observed for the B3 and ZnO cases but to a lesser extent. This slight reduction of V_{OC} can be understood using Eq. (2) [52] where n is the ideality factor, k and T are the Boltzmann constant and the temperature, respectively, and J_l is the current density generated under illumination whereas J_0 is the saturation value in dark. It is well known

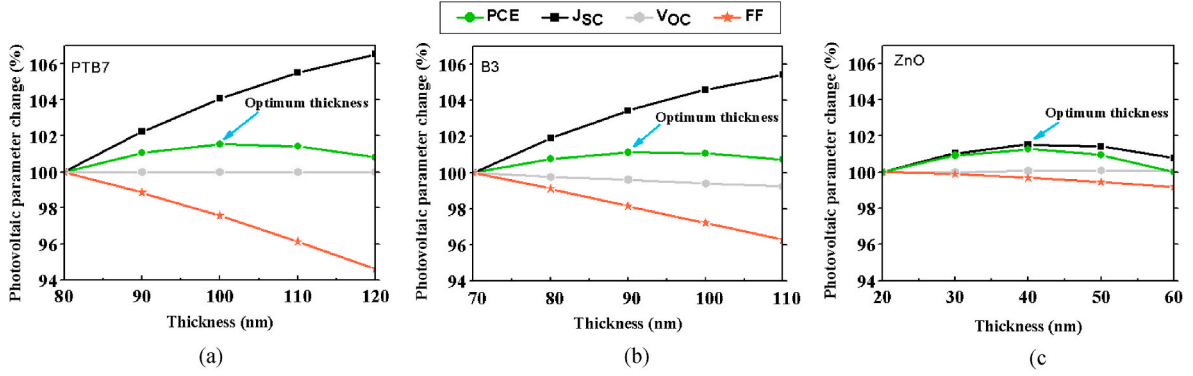


Fig. 10. Development of the characteristic values PCE, J_{sc} , V_{oc} , and FF (Filling Factor) as a function of layer thickness for the three components (a) PTB7, (b) B3, and (c) ZnO, showing the specific optimum thicknesses for the three different layers in a planar solar cell configuration.

that the increase of recombination leads to a J_0 increase, which reduces the V_{oc} .

$$V_{oc} = \frac{nkT}{q} \ln\left(\frac{J_l}{J_0} + 1\right) \quad (2)$$

Further, in order to analyze the effect of the magnitude of the density of trap states in the borinate on the device performance, in the following, the relation between the recombination and trap states is addressed. The charge recombination can be described by the Shockley-Read-Hall model, given by eq. (3) [52].

$$R = \frac{np - n_i^2}{\tau_n \left(p + N_t^* e^{\frac{E_t}{kT}} \right) + \tau_p \left(n + N_t^* e^{\frac{E_t - E_i}{kT}} \right)} \quad (3)$$

where n and p are the concentrations of electrons and holes, respectively. E_t the energy level of trap states, n_i is the intrinsic electron concentration, τ_n and τ_p are the lifetimes of the electron and hole carriers, respectively. The lifetime (τ) of the charge carrier is given by eq. (4) [52].

$$\tau = \frac{1}{\tau^* N_t(E)^* v_{th}} \quad (4)$$

with σ , N_t , and v_{th} the capture cross-section of trap minority carriers, the total trap state density, and the thermal speed energy, respectively. Such Gaussian distributed defect density (N_t) within the bandgap of the semiconductor is described by the following eq. (5) [74].

$$N_t(E) = \frac{N_t}{\sigma\sqrt{2\pi}} * e^{-\frac{(E-E_t)^2}{2\sigma^2}} \quad (5)$$

where N_t is the total trap state density, E_t is the specific energy of the trap Gaussian distribution, and σ^2 is the standard deviation of the trap Gaussian distribution. The considered trap distribution was based on the previously mentioned calibration process.

Fig. 11 shows the effect of the variation of the Gaussian tDOS (from 10^9 cm^{-3} to 10^{12} cm^{-3}) in the B3 borinate, demonstrating that an increase in the defect states density reduces V_{oc} , J_{sc} , and the FF. Regarding the efficiency, it changes by around 3% for each order of magnitude in the tDOS. This is attributed to the fact that the lifetime of the carriers (Eq. (4)) decreases inversely proportionally to the trap density (Eq. (5)), which in turn increases the charge recombination (Eq. (3)).

Finally, it should be mentioned that this proposal structures and analysis can be also used as a design guideline for bulk heterojunction structures since it has been well demonstrated the validity of planar structure models in bulk heterojunction solar cells [36,75]. Besides, there is the important role of internal electric fields in the good performance of such kinds of devices [61], which is consistent with our findings. Note that this band bending effect at the heterojunction can

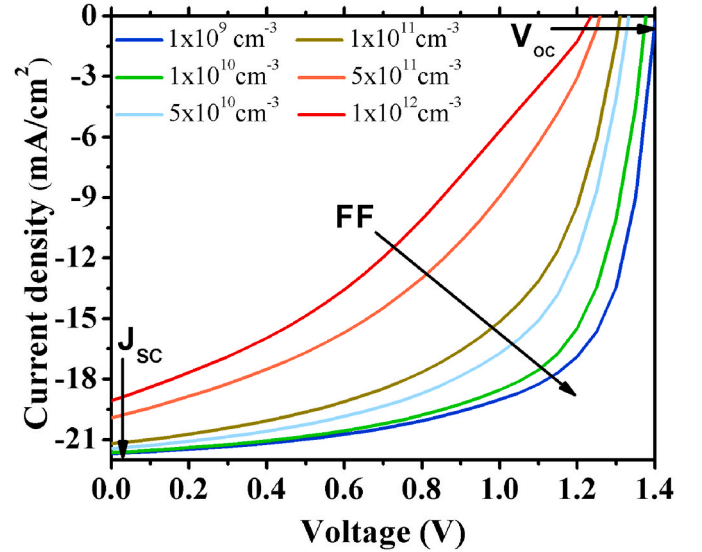


Fig. 11. Effects of trap density variation in B3.

improve the V_{oc} in bilayer organic solar cells [63], which can be attributed to the density of states in the materials of the active layer [76].

4. Conclusions

Based on simple and novel compounds of boron as a ternary material in hybrid solar cells, and by using numerical simulations validated with experimental results, we have shown an optimized efficiency of 15.15% for a PTB7/B3/ZnO ternary device with a planar heterojunction configuration. Specifically, we have tested nine different combinations of a *polymer/borinate/ZnO*-structure hybrid solar cell using three boron compounds with different electrical properties, especially concerning the energy band gap and the trap energy depth (B1, B2, and B3), and three polymers (P3HT, PTB7, and PCPDTBT). Our results also reveal that PTB7 with a thickness of 100 nm, B3 with one of 90 nm, and ZnO with a one of 40 nm are the best thickness values for the optimized solar cell. The highest value of PCE achieved for the PTB7 device can be explained by two factors: i) the higher absorption of the PTB7 when compared to PCPDTBT and ii) its higher built-in electric field with regard to the P3HT device. The electric field induced by PTB7 causes a reduction of charge recombination of two orders of magnitude regarding P3HT. This also explains the difference in the performance between the PTB7/B1/ZnO and PTB7/B2/ZnO devices whose borinates have a similar light absorption. Further, increasing the total trap density of states in the

borinate of the best solar cell structure by one order of magnitude causes an efficiency decrease of around 3%. Finally, we can conclude that our results indicate that borinates are a viable alternative to manufacturing relatively efficient ternary cells with respect to other devices based on more complex molecules and technological processes.

CRedit authorship contribution statement

A. Vázquez: Methodology, Software, Validation, Writing – original draft, Software, Methodology. **A. Castro-Carranza:** Writing – review & editing, Supervision. **M. Rodríguez:** Resources. **J.L. Maldonado:** Writing – review & editing, Conceptualization. **A. Castro-Chacón:** Visualization. **L. García-González:** Writing – review & editing. **J. Hernández-Torres:** Writing – review & editing. **J. Martínez-Castillo:** Writing – review & editing. **L. Zamora-Peredo:** Validation. **J. Gutowski:** Writing – review & editing, Supervision. **J.C. Nolasco:** Writing – review & editing, Supervision, Investigation, Project administration.

Declaration of competing interest

The authors declare that they have no known competing financial interests or personal relationships that could have appeared to influence the work reported in this paper.

Data availability

No data was used for the research described in the article.

Acknowledgment

The support given by CONACYT Mexico, Frontier Science 2019 project CF19-263955 is highly acknowledged. A. Vazquez would like to thank CONACYT for the Ph.D. scholarship to develop this work; Authors thank to Materials and Nanoscience doctoral program of Centro de Investigación en Micro y Nanotecnología (Microna) de Universidad Veracruzana. A. Castro-Carranza, J. Gutowski, and J.C. Nolasco acknowledge GDAPA UNAM PAPIIT, project TA101221, Mexico. J.L. Maldonado thanks LNMG-CONACYT, Mexico. This work has been performed in the framework of the Bremen-Mexican Network on Sustainable Technologies for Environmental Applications (BreMex-STEApS.net).

Appendix A. Supplementary data

Supplementary data to this article can be found online at <https://doi.org/10.1016/j.optmat.2022.112852>.

References

- [1] M. Bhaskaran, S. Sriram, K. Iniewski (Eds.), *Energy Harvesting with Functional Materials and Microsystems*, CRC Press, Boca Raton, 2014. <https://www.routledge.com/Energy-Harvesting-with-Functional-Materials-and-Microsystems-1st-Edition/Bhaskaran-Sriram-Iniewski/p/book/9781466587236>.
- [2] NREL. <https://www.nrel.gov/pv/cell-efficiency.html>, 2021. June 3, 2021.
- [3] I.C. Ghosekar, G.C. Patil, Review on performance analysis of P3HT:PCBM-based bulk heterojunction organic solar cells, *Semicond. Sci. Technol.* 36 (2021), 045005, <https://doi.org/10.1088/1361-6641/abe21b>.
- [4] Z. El Joud, E.M. El-Menyawy, G. Louarn, L. Arzel, M. Morsli, M. Addou, J. C. Bernède, L. Cattin, The effect of the band structure on the Voc value of ternary planar heterojunction organic solar cells based on pentacene, boron subphthalocyanine chloride and different electron acceptors, *J. Phys. Chem. Solid.* 136 (2020), 109142, <https://doi.org/10.1016/j.jpcs.2019.109142>.
- [5] H. Ftouhi, E.M. El-Menyawy, H. Lamkaouane, M. Diani, G. Louarn, J.C. Bernède, M. Addou, L. Cattin, Efficient planar heterojunction based on α -sexithiophene/fullerene through the use of MoO₃/CuI anode buffer layer, *Thin Solid Films* 741 (2022), 139025, <https://doi.org/10.1016/j.tsf.2021.139025>.
- [6] J. Wan, L. Zeng, X. Liao, Z. Chen, S. Liu, P. Zhu, H. Zhu, Y. Chen, All-green solvent-processed planar heterojunction organic solar cells with outstanding power conversion efficiency of 16, *Adv. Funct. Mater.* 32 (2022), 2107567, <https://doi.org/10.1002/adfm.202107567>.
- [7] L. Meng, Y. Zhang, X. Wan, C. Li, X. Zhang, Y. Wang, X. Ke, Z. Xiao, L. Ding, R. Xia, H.-L. Yip, Y. Cao, Y. Chen, Organic and solution-processed tandem solar cells with 17.3% efficiency, *Science* 361 (2018) 1094–1098, <https://doi.org/10.1126/science.aat2612>.
- [8] Y. Chen, Y. Qin, Y. Wu, C. Li, H. Yao, N. Liang, X. Wang, W. Li, W. Ma, J. Hou, From binary to ternary: improving the external quantum efficiency of small-molecule acceptor-based polymer solar cells with a minute amount of fullerene sensitization, *Adv. Energy Mater.* 7 (2017), <https://doi.org/10.1002/aenm.201700328>.
- [9] S. Park, J. Jeong, G. Hyun, M. Kim, H. Lee, Y. Yi, The origin of high PCE in PTB7 based photovoltaics: proper charge neutrality level and free energy of charge separation at PTB7/PC71BM interface, *Sci. Rep.* 6 (2016), 35262, <https://doi.org/10.1038/srep35262>.
- [10] V.A. Trukhanov, D.Y. Paraschuk, Non-fullerene acceptors for organic solar cells, *Polym. Sci. Ser. C* 56 (2014) 72–83, <https://doi.org/10.1134/S181123821401010X>.
- [11] H. Huang, L. Yang, B. Sharma, Recent advances in organic ternary solar cells, *J. Mater. Chem. A* 5 (2017) 11501–11517, <https://doi.org/10.1039/c7ta00887b>.
- [12] L. Duan, N.K. Elumalai, Y. Zhang, A. Uddin, Progress in non-fullerene acceptor based organic solar cells, *Sol. Energy Mater. Sol. Cells* 193 (2019) 22–65, <https://doi.org/10.1016/j.solmat.2018.12.033>.
- [13] L. Ma, S. Zhang, J. Wang, Y. Xu, J. Hou, Recent advances in non-fullerene organic solar cells: from lab to fab, *Chem. Commun.* 56 (2020) 14337–14352, <https://doi.org/10.1039/d0cc05528j>.
- [14] J. Hou, O. Inganäs, R.H. Friend, F. Gao, Organic solar cells based on non-fullerene acceptors, *Nat. Mater.* 17 (2018) 119–128, <https://doi.org/10.1038/NMAT5063>.
- [15] G. Wang, F.S. Melkonyan, A. Facchetti, T.J. Marks, All-polymer solar cells: recent progress, challenges, and prospects, *Angew. Chemie Int. Ed.* 58 (2019) 4129–4142, <https://doi.org/10.1002/anie.201808976>.
- [16] Y. Chang, X. Zhu, K. Lu, Z. Wei, Progress and prospects of thick-film organic solar cells, *J. Mater. Chem. A* 9 (2021) 3125–3150, <https://doi.org/10.1039/d0ta10594e>.
- [17] C. Li, J. Zhou, J. Song, J. Xu, H. Zhang, X. Zhang, J. Guo, L. Zhu, D. Wei, G. Han, J. Min, Y. Zhang, Z. Xie, Y. Yi, H. Yan, F. Gao, F. Liu, Y. Sun, Non-fullerene acceptors with branched side chains and improved molecular packing to exceed 18% efficiency in organic solar cells, *Nat. Energy* 6 (2021) 605–613, <https://doi.org/10.1038/s41560-021-00820-x>.
- [18] T. Yan, W. Song, J. Huang, R. Peng, L. Huang, Z. Ge, 16.67% rigid and 14.06% flexible organic solar cells enabled by ternary heterojunction strategy, *Adv. Mater.* 31 (2019), 1902210, <https://doi.org/10.1002/adma.201902210>.
- [19] Q. Liu, Y. Jiang, K. Jin, J. Qin, J. Xu, W. Li, J. Xiong, J. Liu, Z. Xiao, K. Sun, S. Yang, X. Zhang, L. Ding, 18% Efficiency organic solar cells, *Sci. Bull.* 65 (2020) 272–275, <https://doi.org/10.1016/j.scib.2020.01.001>.
- [20] Y. Cui, Y. Xu, H. Yao, P. Bi, L. Hong, J. Zhang, Y. Zu, T. Zhang, J. Qin, J. Ren, Z. Chen, C. He, X. Hao, Z. Wei, J. Hou, Single-junction organic photovoltaic cell with 19% efficiency, *Adv. Mater.* 33 (2021), 2102420, <https://doi.org/10.1002/adma.202102420>.
- [21] J.C. Nolasco, J.W. Ryan, M. Rodríguez, A. Castro-Carranza, J.L. Maldonado, G. Ramos-Ortiz, O. Barbosa-García, J. Gutowski, E. Palomares, J. Parisi, Organoboron donor- π -acceptor chromophores for small-molecule organic solar cells, *J. Mater. Sci. Mater. Electron.* 29 (2018) 16410–16415, <https://doi.org/10.1007/s10854-018-9732-6>.
- [22] B.M. Squeo, L. Ganzer, T. Virgili, M. Pasini, BODIPY-based molecules, a platform for photonic and solar cells, *Molecules* 26 (2020) 153, <https://doi.org/10.3390/molecules26010153>.
- [23] A.N. Bismillah, I. Aprahamian, Fundamental studies to emerging applications of pyrrole-BF₂ (BOPHY) fluorophores, *Chem. Soc. Rev.* 50 (2021) 5631–5649, <https://doi.org/10.1039/D1CS00122A>.
- [24] I.A. Skvortsov, U.P. Kovkova, Y.A. Zhabanov, I.A. Khodov, N.V. Somov, G. L. Pakhomov, P.A. Stuzhin, Subphthalocyanine-type dye with enhanced electron affinity: effect of combined azasubstitution and peripheral chlorination, *Dyes Pigments* 185 (2021), 108944, <https://doi.org/10.1016/j.dyepig.2020.108944>.
- [25] M. Rodríguez, R. Castro-Beltrán, G. Ramos-Ortiz, J.L. Maldonado, N. Farfán, O. Domínguez, J. Rodríguez, R. Santillan, M.A. Meneses-Nava, O. Barbosa-García, J. Peon, Synthesis and third-order nonlinear optical studies of a novel four-coordinated organoboron derivative and a bidentate ligand, *Synth. Met.* 159 (2009) 1281–1287, <https://doi.org/10.1016/j.synthmet.2009.02.027>.
- [26] M. Rodríguez, J.L. Maldonado, G. Ramos-Ortiz, J.F. Lamère, P.G. Lacroix, N. Farfán, M.E. Ochoa, R. Santillan, M.A. Meneses-Nava, O. Barbosa-García, K. Nakatani, Synthesis and non-linear optical characterization of novel boronate derivatives of cinnamaldehyde, *New J. Chem.* 33 (2009) 1693–1702, <https://doi.org/10.1039/b820435g>.
- [27] J.-A. Del-Oso, J.-L. Maldonado, G. Ramos-Ortiz, M. Rodríguez, M. Güizado-Rodríguez, J. Escalante, B.A. Frontana-Urbe, E. Pérez-Gutiérrez, R. Santillan, New polythiophene derivatives and enhanced photovoltaic effect by a boron compound blended with them in OPVs cells, *Synth. Met* 196 (2014) 83–91, <https://doi.org/10.1016/j.synthmet.2014.07.019>.
- [28] A. Soultati, A. Verykios, S. Panagiotakis, K.K. Armadorou, M.I. Haider, A. Kaltzoglou, C. Drivas, A. Fakhreddin, X. Bao, C. Yang, A.R.B.M. Yusoff, E. K. Evangelou, I. Petsalakis, S. Kennou, P. Falaras, K. Yannakopoulou, G. Pistolis, P. Argitis, M. Vasilopoulou, Suppressing the photocatalytic activity of zinc oxide electron-transport layer in nonfullerene organic solar cells with a pyrene-bodipy interlayer, *ACS Appl. Mater. Interfaces* 12 (2020) 21961–21973, <https://doi.org/10.1021/acami.0c03147>.
- [29] W.X. Liu, J.N. Yao, C.L. Zhan, Tailoring the photophysical and photovoltaic properties of boron-difluorodipyromethene dimers, *Chin. Chem. Lett.* 28 (2017) 875–880, <https://doi.org/10.1016/j.ccl.2017.01.013>.

- [30] R. Varache, C. Leendertz, M.E. Gueunier-Farret, J. Haschke, D. Muñoz, L. Korte, Investigation of selective junctions using a newly developed tunnel current model for solar cell applications, *Sol. Energy Mater. Sol. Cells* 141 (2015) 14–23, <https://doi.org/10.1016/j.solmat.2015.05.014>.
- [31] W. Abdelaziz, A. Zekry, A. Shaker, M. Abouelatta, Numerical study of organic graded bulk heterojunction solar cell using SCAPS simulation, *Sol. Energy* 211 (2020) 375–382, <https://doi.org/10.1016/j.solener.2020.09.068>.
- [32] J.A. Carr, S. Chaudhary, The identification, characterization and mitigation of defect states in organic photovoltaic devices: a review and outlook, *Energy Environ. Sci.* 6 (2013) 3414, <https://doi.org/10.1039/c3ee41860j>.
- [33] S. Olthof, S. Mehraeen, S.K. Mohapatra, S. Barlow, V. Coropceanu, J.-L. Brédas, S. R. Marder, A. Kahn, Ultralow doping in organic semiconductors: evidence of trap filling, *Phys. Rev. Lett.* 109 (2012), 176601, <https://doi.org/10.1103/PhysRevLett.109.176601>.
- [34] J.A. Carr, S. Chaudhary, The identification, characterization and mitigation of defect states in organic photovoltaic devices: a review and outlook, *Energy Environ. Sci.* 6 (2013) 3414, <https://doi.org/10.1039/c3ee41860j>.
- [35] J.C. Nolasco, A. Sánchez-Díaz, R. Cabré, J. Ferré-Borrull, L.F. Marsal, E. Palomares, J. Pallarès, Relation between the barrier interface and the built-in potential in pentacene/C60 solar cell, *Appl. Phys. Lett.* 97 (2010), 013305, <https://doi.org/10.1063/1.3456393>.
- [36] J.C. Nolasco, A. Castro-Carranza, Y.A. León, C. Briones-Jurado, J. Gutowski, J. Parisi, E. von Hauff, Understanding the open circuit voltage in organic solar cells on the basis of a donor-acceptor abrupt (p-n++) heterojunction, *Sol. Energy* 184 (2019) 610–619, <https://doi.org/10.1016/j.solener.2019.04.031>.
- [37] P.W.M. Blom, V.D. Mihaileti, L.J.A. Koster, D.E. Markov, Device physics of polymer/fullerene bulk heterojunction solar cells, *Adv. Mater.* 19 (2007) 1551–1566, <https://doi.org/10.1002/adma.200601093>.
- [38] S.-W. Liu, W.-C. Su, C.-C. Lee, C.-F. Lin, S.-C. Yeh, C.-T. Chen, J.-H. Lee, Comparison of short and long wavelength absorption electron donor materials in C60-based planar heterojunction organic photovoltaics, *Org. Electron.* 13 (2012) 2118–2129, <https://doi.org/10.1016/j.orgel.2012.06.006>.
- [39] N. Mendil, M. Daoudi, Z. Berkai, A. Belghachi, Charge carrier mobility behavior in the SubPc/C60 planar heterojunction, *Z. Naturforsch.* 73 (2018) 1047–1052, <https://doi.org/10.1515/zna-2018-0142>.
- [40] K. Kudo, T. Saraya, S. Kuniyoshi, K. Tanaka, Electrical characterization of C 60 evaporated films using MOS structure, *Mol. Cryst. Liq. Cryst. Sci. Technol. Mol. Cryst. Liq. Cryst.* 267 (1995) 423–428, <https://doi.org/10.1080/10587259508034026>.
- [41] H. Frankenstein, C.Z. Leng, M.D. Losego, G.L. Frey, Atomic layer deposition of ZnO electron transporting layers directly onto the active layer of organic solar cells, *Org. Electron.* 64 (2019) 37–46, <https://doi.org/10.1016/j.orgel.2018.10.002>.
- [42] Z. Bahrami, A. Salehi, A.M. Eyyaraghi, AMPS-1D modelling of P3HT/PCBM bilayer and BHJ organic solar cell, in: 2019 27th Iran. Conf. Electr. Eng., IEEE, 2019, pp. 41–45, <https://doi.org/10.1109/IranianCEE.2019.8786641>.
- [43] N. Singh, A. Agarwal, M. Agarwal, Numerical simulation of highly efficient lead-free all-perovskite tandem solar cell, *Sol. Energy* 208 (2020) 399–410, <https://doi.org/10.1016/j.solener.2020.08.003>.
- [44] J.C. Nolasco, R. Cabré, J. Ferré-Borrull, L.F. Marsal, M. Estrada, J. Pallarès, Extraction of poly (3-hexylthiophene) (P3HT) properties from dark current voltage characteristics in a P3HT/n-crystalline-silicon solar cell, *J. Appl. Phys.* 107 (2010), 044505, <https://doi.org/10.1063/1.3296294>.
- [45] P.T.B.7 Sigma-Aldrich. <https://www.sigmaaldrich.com/catalog/product/aldrich/772410?lang=en®ion=US>, 2020, September 18, 2020.
- [46] F. Azri, A. Meftah, N. Sengouga, A. Meftah, Electron and hole transport layers optimization by numerical simulation of a perovskite solar cell, *Sol. Energy* 181 (2019) 372–378, <https://doi.org/10.1016/j.solener.2019.02.017>.
- [47] M. Samiee, P. Joshi, D. Aidarkhanov, V. Dalal, Measurement of defect densities and Urbach energies of tail states in PTB7 solar cells, *Appl. Phys. Lett.* 105 (2014), 133511, <https://doi.org/10.1063/1.4896782>.
- [48] S. Yadav, S.S.K. Iyer, Building a planar single and binary blend stack ternary organic solar cells, *Flex. Print. Electron.* 4 (2019), 034003, <https://doi.org/10.1088/2058-8585/ab35f8>.
- [49] W. Mech, J. Borysiuk, A. Wincukiewicz, R. Bożek, P. Trautman, M. Tokarczyk, M. Kamińska, K. Korona, Influence of active layer processing on electrical properties and efficiency of polymer-fullerene organic solar cells, *Acta Phys. Pol., A* 136 (2019) 579–585, <https://doi.org/10.12693/APhysPolA.136.579>.
- [50] B.A. Gregg, Charged defects in soft semiconductors and their influence on organic photovoltaics, *Soft Matter* 5 (2009) 2985, <https://doi.org/10.1039/b905722f>.
- [51] S. Abdelaziz, A. Zekry, A. Shaker, M. Abouelatta, Investigation of lead-free MASnI3-MASnBr2 tandem solar cell: numerical simulation, *Opt. Mater.* 123 (2022), 111893, <https://doi.org/10.1016/j.optmat.2021.111893>.
- [52] W. Abdelaziz, A. Shaker, M. Abouelatta, A. Zekry, Possible efficiency boosting of non-fullerene acceptor solar cell using device simulation, *Opt. Mater.* 91 (2019) 239–245, <https://doi.org/10.1016/j.optmat.2019.03.023>.
- [53] S. Abdelaziz, A. Zekry, A. Shaker, M. Abouelatta, Investigating the performance of formamidinium tin-based perovskite solar cell by SCAPS device simulation, *Opt. Mater.* 101 (2020), 109738, <https://doi.org/10.1016/j.optmat.2020.109738>.
- [54] H.J. Snaith, How should you measure your excitonic solar cells? *Energy Environ. Sci.* 5 (2012) 6513, <https://doi.org/10.1039/c2ee03429h>.
- [55] C. Tong, W. Ji, D. Li, A. Mei, Y. Hu, Y. Rong, H. Han, Modeling the edge effect for measuring the performance of mesoscopic solar cells with shading masks, *J. Mater. Chem. A* 7 (2019) 10942–10948, <https://doi.org/10.1039/C9TA02459J>.
- [56] X. Liu, Y. Yan, Y. Yao, Z. Liang, Ternary blend strategy for achieving high-efficiency organic solar cells with nonfullerene acceptors involved, *Adv. Funct. Mater.* 28 (2018), 1802004, <https://doi.org/10.1002/adfm.201802004>.
- [57] B. Usmani, R. Ranjan, Prateek, S.K. Gupta, R.K. Gupta, K.S. Nalwa, A. Garg, PTB7-Th Inverted, PC71BM organic solar cells with 11.8% PCE via incorporation of gold nanoparticles in ZnO electron transport layer, *Sol. Energy* 214 (2021) 220–230, <https://doi.org/10.1016/j.solener.2020.11.071>.
- [58] C. Zhou, R. Hu, Y. Liu, M.-M. Huo, L. Li, J. Yu, Effect of colloid aggregation characteristic on ZnO interface layer and photovoltaic performance of polymer solar cells, *Org. Electron.* 83 (2020), 105753, <https://doi.org/10.1016/j.orgel.2020.105753>.
- [59] D. Duché, F. Bencheikh, S. Ben Dkhil, M. Gaceur, N. Berton, O. Margeat, J. Ackermann, J.J. Simon, L. Escoubas, Optical performance and color investigations of hybrid solar cells based on P3HT:ZnO, PCPDTBT:ZnO, PTB7:ZnO and DTS(PTTh2):ZnO, *Sol. Energy Mater. Sol. Cells* 126 (2014) 197–204, <https://doi.org/10.1016/j.solmat.2014.03.049>.
- [60] S. Izawa, N. Shintaku, M. Hiramoto, Effect of band bending and energy level alignment at the donor/acceptor interface on open-circuit voltage in organic solar cells, *J. Phys. Chem. Lett.* 9 (2018) 2914–2918, <https://doi.org/10.1021/acs.jpcclett.8b01134>.
- [61] I. Lange, J.C. Blakesley, J. Frisch, A. Vollmer, N. Koch, D. Neher, Band bending in conjugated polymer layers, *Phys. Rev. Lett.* 106 (2011), 216402, <https://doi.org/10.1103/PhysRevLett.106.216402>.
- [62] R. Saive, S-shaped current–voltage characteristics in solar cells: a review, *IEEE J. Photovoltaics* 9 (2019) 1477–1484, <https://doi.org/10.1109/JPHOTOV.2019.2930409>.
- [63] S. Izawa, N. Shintaku, M. Hiramoto, Effect of band bending and energy level alignment at the donor/acceptor interface on open-circuit voltage in organic solar cells, *J. Phys. Chem. Lett.* 9 (2018) 2914–2918, <https://doi.org/10.1021/acs.jpcclett.8b01134>.
- [64] R. Sharma, F. Alam, A.K. Sharma, V. Dutta, S.K. Dhawan, ZnO anchored graphene hydrophobic nanocomposite-based bulk heterojunction solar cells showing enhanced short-circuit current, *J. Mater. Chem. C* 2 (2014) 8142–8151, <https://doi.org/10.1039/C4TC01056F>.
- [65] R. Liyakath, B. Ramaraj, P.-K. Shin, K. Santhakumar, Restructuring and interlayer phenomenon on tandem architecture to improve organic solar cell behaviour, *J. Mater. Sci. Mater. Electron.* 32 (2021) 7729–7738, <https://doi.org/10.1007/s10854-021-05491-8>.
- [66] A.M. Poe, A.M. Della Pelle, A. V. Subrahmanyam, W. White, G. Wantz, S. Thayumanavan, Small molecule BODIPY dyes as non-fullerene acceptors in bulk heterojunction organic photovoltaics, *Chem. Commun.* 50 (2014) 2913–2915, <https://doi.org/10.1039/C3CC49648A>.
- [67] S.K. Sarkar, L.J. Kang, U.K. Pandey, C.K. Luscombe, P. Thilagar, Triarylborane-BODIPY conjugate: an efficient non-fullerene electron acceptor for bulk heterojunction organic solar cell, *Sol. Energy* 230 (2021) 242–249, <https://doi.org/10.1016/j.solener.2021.10.048>.
- [68] B. Qi, J. Wang, Open-circuit voltage in organic solar cells, *J. Mater. Chem.* 22 (2012), 24315, <https://doi.org/10.1039/c2jm33719c>.
- [69] Y. Wang, B. Jia, J. Wang, P. Xue, Y. Xiao, T. Li, J. Wang, H. Lu, Z. Tang, X. Lu, F. Huang, X. Zhan, High-efficiency perovskite quantum dot hybrid nonfullerene organic solar cells with near-zero driving force, *Adv. Mater.* 32 (2020) 1–8, <https://doi.org/10.1002/adma.202002066>.
- [70] C.-M. Oh, J. Lee, S.H. Park, I.-W. Hwang, Enhanced charge separation in ternary bulk-heterojunction organic solar cells by fullerenes, *J. Phys. Chem. Lett.* (2021) 6418–6424, <https://doi.org/10.1021/acs.jpcclett.1c01496>.
- [71] R. Singh, S.C. Shin, H. Lee, M. Kim, J.W. Shim, K. Cho, J.J. Lee, Ternary blend strategy for achieving high-efficiency organic photovoltaic devices for indoor applications, *Chem. Eur. J.* 25 (2019) 6154–6161, <https://doi.org/10.1002/chem.2019000041>.
- [72] Y. Cui, H. Yao, J. Zhang, T. Zhang, Y. Wang, L. Hong, K. Xian, B. Xu, S. Zhang, J. Peng, Z. Wei, F. Gao, J. Hou, Over 16% efficiency organic photovoltaic cells enabled by a chlorinated acceptor with increased open-circuit voltages, *Nat. Commun.* 10 (2019) 2515, <https://doi.org/10.1038/s41467-019-10351-5>.
- [73] H. Zhang, H. Yao, J. Hou, J. Zhu, J. Zhang, W. Li, R. Yu, B. Gao, S. Zhang, J. Hou, Over 14% efficiency in organic solar cells enabled by chlorinated nonfullerene small-molecule acceptors, *Adv. Mater.* 30 (2018) 1–7, <https://doi.org/10.1002/adma.201800613>.
- [74] R. Stangl, C. Leendertz, in: *General Principles of Solar Cell Simulation and Introduction to AFORS-HET*, 2012, pp. 445–458, https://doi.org/10.1007/978-3-642-22275-7_13.
- [75] B. Ecker, J.C. Nolasco, J. Pallarès, L.F. Marsal, J. Posdorfer, J. Parisi, E. Von Hauff, Degradation effects related to the hole transport layer in organic solar cells, *Adv. Funct. Mater.* 21 (2011) 2705–2711, <https://doi.org/10.1002/adfm.201100429>.
- [76] N. Shintaku, M. Hiramoto, S. Izawa, Doping for controlling open-circuit voltage in organic solar cells, *J. Phys. Chem. C* 122 (2018) 5248–5253, <https://doi.org/10.1021/acs.jpcc.7b12203>.